Adaptive coupling of reduced basis modeling and Kriging based active learning methods for reliability analyses

Morgane Menz, Christian Gogu, Sylvain Dubreuil, Nathalie Bartoli, Jérôme Morio

Adaptive coupling of reduced basis modeling and Kriging based active learning methods for reliability analyses

Morgane Menz[a,b], Christian Gogu[a], Sylvain Dubreuil[b], Nathalie Bartoli[b], Jérôme Morio[b]

[a] *Université de Toulouse, UPS, CNRS, INSA, Mines Albi, ISAE, Institut Clément Ader (ICA), 3 rue Caroline Aigle, 31400 Toulouse, France*
[b] *ONERA/DTIS, Université de Toulouse, F-31055 Toulouse, France*

Abstract

Running a reliability analysis on engineering problems involving complex numerical models can be computationally very expensive. Hence, advanced methods are required to reduce the number of calls to the expensive computer codes. Adaptive sampling based reliability analysis methods are one promising way to reduce computational costs. Reduced order modelling is another one. In order to further reduce the numerical costs of Kriging based adaptive sampling approaches, the idea developed in this paper consists in coupling both approaches by adaptively deciding whether to use reduced-basis solutions in place of full numerical solutions whenever the performance function needs to be assessed. Thus, a method combining such adaptive sampling based reliability analyses and reduced basis modeling is proposed using on an efficient coupling criterion. The proposed method enabled significant computational cost reductions, while ensuring accurate estimations of failure probabilities.

Keywords: `Reliability analysis, Kriging, Adaptive approaches, Finite elements, Reduced order modeling, Reduced basis`

1. Introduction

Reliability analyses are an efficient tool to deal with the numerous uncertainties present in engineering systems and thus determine the probability of failure of these systems. Many recent developments in this field seek to address

increasingly complex numerical models, involving large physical and stochastic dimensions or even complex mechanical behaviors.

Generally speaking, a system failure mode is determined by a criterion defined by a so-called performance function. By convention, a negative value of this function corresponds to the failure of the system, whereas a positive value corresponds to an operational system. The limit between the failure and the safety domain is named limit state and corresponds to a null performance function. It thus allows the calculation of the probability of failure.

Several reliability analysis techniques exist to estimate the probability of failure such as analytic approximations (FORM/SORM), sampling methods [1], surrogate-based reliability analysis methods which can be adaptive or not. Adaptive approaches have been proposed in particular for Kriging surrogates [2, 3, 4, 5, 6, 7, 8, 9], support vector machines [10, 11], polynomial-chaos-based Kriging in [12]. For a fixed sampling technique, the probability of failure is obtained by a classification of the samples, which is usually done by evaluating the numerical model at the corresponding samples. However, sometimes it may not be necessary to compute the full numerical model for all the samples, as many phenomena are very well described by a few dominant modes that can be accurately estimated based on adjacent samples. This is the basic idea of model order reduction approaches, which are used to reduce a system's complexity while best preserving the system's response behaviour. In this paper, we focus on the model order reduction techniques known as reduced basis approaches or reduced order models by projection [13, 14]. These methods rely on the projection of the governing equations of the physical model involved onto a subspace of greatly reduced dimensionality compared to the initial space. Hence the resolution of the projected system involves a significantly reduced computational cost. Following this concept, reduced basis techniques have already been combined with several reliability analysis techniques such as first or second-order reliability method or sampling based methods (i.e. Monte Carlo Simulations or even Importance Sampling) [15, 16, 17, 18] and were shown to be able to lead to substantial computational savings. Presently, some of the most promising

methods for reliability analysis are the ones based on an adaptive sampling approach. Kriging-based adaptive sampling methods which are also the object of this work, consist in building a Kriging surrogate model (Gaussian process interpolation) [19, 20] of the performance function and using the uncertainty structure of Kriging to enrich iteratively this surrogate model. At each iteration of the algorithm, the best candidate for the next simulation is selected on the basis of a learning criterion and computed to increase the accuracy of the Kriging metamodel. This learning criterion is built to learn the limit state.

Several adaptive methods have been proposed such as the efficient global reliability analysis (EGRA) by Bichon et. al [4] or Active learning reliability method combining Kriging and Monte Carlo Simulations (AK-MCS) by Echard et. al [21]. Other methods have also been presented to address specific problems such as small failure probabilities (rare events) estimations [3, 22, 23, 24, 25, 7, 26] , multiple failure regions problems [27, 28, 29, 30] or systems failure probabilities assessment [6, 31, 5, 2, 9, 32].

In practice algorithms will enrich the metamodel in the vicinity of the currently known limit state and also explore the design space in less known areas, i.e. areas where the metamodel variance is high. To motivate our present work we can note that points in the vicinity of the limit state might be close to other points already evaluated and consequently the use of reduced-order solutions at these points are likely to have good accuracy while accelerating the method. Enrichment points in regions of high variance could also potentially benefit from reduced basis modelling, since these points can initially be calculated with the lower accuracy associated with reduced basis models, which may be enough to clarify the performance function's behaviour in these areas.

Accordingly the objective of this paper is to propose a reliability analysis method based on the coupling of adaptive sampling and reduced basis approaches. The proposed approach can thus be seen as an adaptive fidelity reliability analysis [33] for the specific problems that are suitable for reduced basis modelling. Indeed, the reduced basis model is a low-fidelity model with increasing fidelity as the reduced basis is enriched. Hence, low-fidelity solutions

can be used when they are sufficiently accurate, or if it is necessary the fidelity can be increased by using the high-fidelity model. The main challenge for setting up such an approach resides in defining an appropriate coupling criterion, based on which to decide whether the reduced basis models can be used or whether the accuracy of the full numerical model is required. Different criteria based on a residual based error estimator will be investigated: one quite simple criterion but which can sometimes have poor accuracy and a preconditioning based criterion, which can generally improve accuracy. The rest of the article is organized as follows. We present in Section 2 the problem statement. In Section 3 we provide a presentation of methods on which we build on: adaptive sampling based reliability analysis and, more precisely, the AK-MCS algorithm [21]. Section 3 also introduces the reduced-basis approach used in the present article. In Section 4 the new method combining adaptive sampling techniques and reduced-basis modeling is presented. First, we describe the overall framework of the proposed approach. Then two implementations for the coupling of the algorithm AK-MCS with reduced-basis modeling are proposed, based on different coupling criteria. In Section 5 two application examples are considered. The first application concerns a reliability analysis on a thermal problem related to a regeneretivly cooled combustion chamber. The second one is the estimation of the probability of failure of a laminated composite open hole plate based on the Tsaï-Hill failure criterion. The performance of the proposed method is compared to the AK-MCS results and computational gains assessed.

2. Problem statement

This paper deals with reliability analyses involving certain numerically expensive models, specifically linear systems obtained by finite element discretization (e.g. in structural mechanics, heat transfer, etc). Let $x_1, ..., x_m$ be the m uncertain parameters that are inputs to the finite element model. These parameters are modeled by an absolutely continuous random vector $\boldsymbol{X}$ of random variables X_i, $i = 1, \ldots, m$ characterized by a probability distribution with prob-

ability density function $f_{\boldsymbol{X}}$. The output of the numerical model $Y(\boldsymbol{X})$ is then also a random variable. After finite element discretization of the equilibrium equation and the application of boundary conditions the following linear system of n degrees of freedom is typically obtained:

$$\boldsymbol{K}(\boldsymbol{x})\boldsymbol{u}(\boldsymbol{x}) = \boldsymbol{F}(\boldsymbol{x}) \tag{1}$$

where $\boldsymbol{K}(\boldsymbol{x})$ is an $n \times n$ matrix (called stiffness matrix in structural mechanics), $\boldsymbol{u}(\boldsymbol{x}) \in \mathbb{R}^n$ the vector of the unknown state variables (e.g. displacements in structural mechanics, temperatures in heat exchange, etc) and $\boldsymbol{F}(\boldsymbol{x}) \in \mathbb{R}^n$ the vector of loadings (e.g. applied forces in structural mechanics, heat fluxes in heat transfer). In the context of reliability, the output of interest is the performance function $G(\boldsymbol{x})$, which is considered here dependent on the state variable $\boldsymbol{u}(\boldsymbol{x})$, solution of the finite element model:

$$G(\boldsymbol{x}) = G(\boldsymbol{u}(\boldsymbol{x}), \boldsymbol{x}) \tag{2}$$

The performance function $G : \mathbb{R}^m \to \mathbb{R}$ characterizes the failure of a structure. Hence the domain of failure reads $\mathcal{D}_f = \{\boldsymbol{x} \in \mathbb{R}^m, G(\boldsymbol{x}) \leq 0\}$,the domain of safety reads $\{\boldsymbol{x} \in \mathbb{R}^m, G(\boldsymbol{x}) > 0\}$ and the limit state is $\{\boldsymbol{x} \in \mathbb{R}^m, G(\boldsymbol{x}) = 0\}$. The failure probability P_f is then defined as:

$$P_f = \int_{\mathbb{R}^m} \mathbb{1}_{G(\boldsymbol{x})\leq 0} f_{\boldsymbol{X}}(\boldsymbol{x}) d\boldsymbol{x} \tag{3}$$

Several methods exist to obtain an estimation of this probability. One of the simplest method is Monte Carlo Simulation (MCS). It consists in simulating a random independent and identically distributed sample $\boldsymbol{x}^1, ..., \boldsymbol{x}^{n_{MC}}$ of size n_{MC} with distribution $f_{\boldsymbol{X}}$ and then classifying this population given the value taken by the performance function. An estimation $\hat{P}_f$ of the failure probability P_f is then given by:

$$\hat{P}_{f\,MC} = \frac{1}{n_{MC}} \sum_{i=1}^{n_{MC}} \mathbb{1}_{G(\boldsymbol{x})\leq 0}(\boldsymbol{x}^i) \tag{4}$$

The following estimation of the coefficient of variation (COV) can be used to quantify the uncertainty of the estimated failure probability:

$$\widehat{COV}_{P_f\,MC} = \sqrt{\frac{(1-\hat{P}_{f\,MC})}{n_{MC}\hat{P}_{f\,MC}}} \tag{5}$$

It can be seen in Eq. (5) that for a failure probability of 10^{-n}, 10^{n+2} simulations are needed to obtain an estimated coefficient of variation of about 10%. The computational cost may thus be very important for computationally expensive functions $G(\boldsymbol{x})$. In the next section, an alternative approach based on adaptive sampling is presented.

3. Adaptive sampling based reliability analysis methods and Reduced-Basis Modeling

3.1. Reliability analysis using a Kriging surrogate model

Sampling based classification methods need a lot of simulations to estimate the failure probability. In order to avoid to evaluate a complex performance function $G(\boldsymbol{x})$ on a whole Monte Carlo population, an approximation by a surrogate model of this function $\hat{G}(\boldsymbol{x})$ can be used instead. However the accuracy of the surrogate model needs to be controlled in the regions near the limit state. For this purpose, Kriging based adaptive sampling methods allow to construct and enrich a Kriging metamodel by using the uncertainty structure of this type of surrogate models to adaptively add learning points in regions that contribute significantly to the probability of failure estimate. More specifically, these methods use learning functions to select the best point to evaluate i.e. the one which would improve the metamodel in the vicinity of the limit state.

3.1.1. The Kriging surrogate model

Kriging, introduced in geostatistics by Krige [34] and formalized later by Georges Matheron [35], is a method of interpolation in which the interpolated function is modeled by a Gaussian process. A Kriging or Gaussian Process

(GP) [19] $\mathcal{G}$ is fully characterized by the Kriging mean $m(\boldsymbol{x})$ and a kernel (or covariance function) $k(\cdot,\cdot)$ and can be defined as:

$$\mathcal{G}(\boldsymbol{x}) = m(\boldsymbol{x}) + Z(\boldsymbol{x}) \tag{6}$$

with:

- the Kriging mean $m(\boldsymbol{x}) = \boldsymbol{\Phi}(\boldsymbol{x})\boldsymbol{\beta}$ with $\boldsymbol{\Phi}(\boldsymbol{x})$ a basis functions vector and $\boldsymbol{\beta}$ the associated regression coefficients.
- $Z(\boldsymbol{x})$ a stationary zero mean Gaussian process with the variance σ_Z^2 such that the kernel defining the Kriging is

  $$k(\boldsymbol{v},\boldsymbol{w}) = \mathrm{cov}(\mathcal{G}(\boldsymbol{v}),\mathcal{G}(\boldsymbol{w})) = \sigma_Z \Psi(\boldsymbol{v},\boldsymbol{w},\boldsymbol{\theta}),$$

  Ψ being a user defined correlation function type.

Finally, the hyperparameters $\boldsymbol{\theta}$, σ_Z, $\boldsymbol{\beta}$ must be estimated to approximate the response for any unknown point of the domain. For a fixed kernel type, several techniques exist to obtain the optimal values of these hyperparameters, for example by Maximum Likelihood Estimation [36] or cross-validation [19].

The prior distribution of $\mathcal{G}$ is considered to be Gaussian. Hence, the posterior distribution of $\mathcal{G}$ knowing the observations $\{\boldsymbol{y} = G(\boldsymbol{x}_{doe}), \boldsymbol{x}_{doe} = (\boldsymbol{x}^1, ..., \boldsymbol{x}^n)\}$ is Gaussian $\mathcal{G}|y, \boldsymbol{x}_{doe} \sim GP(\mu_{\hat{G}}(\cdot), \sigma^2_{\hat{G}}(\cdot))$. The mean and variance of the Kriging predictor $\hat{G}(\boldsymbol{x}^*)$ of the response $G(\boldsymbol{x}^*)$ at a point $\boldsymbol{x}^*$ are then given by the expressions:

$$\mu_{\hat{G}}(\boldsymbol{x}^*) = m(\boldsymbol{x}^*) + \boldsymbol{k}(\boldsymbol{x}^*)\boldsymbol{C}^{-1}(\boldsymbol{y} - m(\boldsymbol{x}^*)\boldsymbol{1}) \tag{7}$$

$$\sigma^2_{\hat{G}}(\boldsymbol{x}^*) = k(\boldsymbol{x}^*,\boldsymbol{x}^*) - \boldsymbol{k}(\boldsymbol{x}^*)^T\boldsymbol{C}^{-1}\boldsymbol{k}(\boldsymbol{x}^*) \tag{8}$$

where $\boldsymbol{k}(\boldsymbol{x}^*) = (k(\boldsymbol{x}^*,\boldsymbol{x}^1),\ldots,k(\boldsymbol{x}^*,\boldsymbol{x}^n))^T$ and $\boldsymbol{C} := (k(x^i,x^j))_{i,j}$ is the covariance matrix between the observations.

In the following section, the adaptive sampling reliability analysis method AK-MCS, which combines Kriging and Monte Carlo based Simulation, will be presented.

3.1.2. AK-MCS

The active learning reliability method combining Kriging and Monte Carlo Simulation (AK-MCS) is an adaptive reliability estimation method proposed by Echard et al. [21], based on the interpolation of the performance function by Kriging together with the use of a specific learning function and on the Monte Carlo method. This method aims to classify a Monte Carlo population S without evaluating each sample with the numerically expensive performance function. The different stages of AK-MCS are summarized in Fig. 1 and described below:

1. Generation of an initial Monte Carlo population S of n_{MC} samples.
2. Initial Design of Experiments (DoE) D of n_D samples defined using sampling methods such as Latin Hypercube Sampling (LHS). Here we generate the Latin Hypercube sampling using the class LHSExperiment of the Python library Openturns [37], which takes into account the actual variables distributions. The performance function $G(\boldsymbol{x})$ is then evaluated for the n_D samples.
3. Construction of a Kriging metamodel $\hat{G}(\boldsymbol{x})$ of the performance function $G(\boldsymbol{x})$ on the DoE.
4. Estimation of the failure probability P_f on the Monte Carlo population S according to the following equation:

$$\hat{P}_{f\,AK-MCS} \approx \frac{n_{\hat{G}\leq 0}}{n_{MC}} \tag{9}$$

where $n_{\hat{G}\leq 0}$ corresponds to the number of samples of S in the domain of failure.

5. The learning function $U(\boldsymbol{x})$ given in Eq. (10) is evaluated on the whole population S to find the best candidate to evaluate for enriching the Kriging metamodel.

$$U(\boldsymbol{x}) = \frac{|\mu_{\hat{G}}(\boldsymbol{x})|}{\sigma_{\hat{G}}(\boldsymbol{x})} \tag{10}$$

with $\mu_{\hat{G}}(\boldsymbol{x})$ and $\sigma_{\hat{G}}(\boldsymbol{x})$ respectively the mean and standard deviation of the Kriging model of $\hat{G}(\boldsymbol{x})$ (see Eq. (7) and Eq. (8)).

6. If the learning stopping criterion defined by Eq. (11) is fullfiled the meta-model is considered sufficiently accurate for the population S and the active learning is stopped. Then the algorithm goes to step 8. Otherwise, the algorithm goes to step 7.

$$\min_{\boldsymbol{x} \in S} U(\boldsymbol{x}) \geq 2 \tag{11}$$

7. The performance function is computed on the sample $\boldsymbol{x}^*$ minimizing the learning function $U(\boldsymbol{x})$ and the DoE is enriched with this new point $\boldsymbol{x}^*$. Then the algorithm goes back to step 3.

8. The estimated value of the coefficient of variation (COV) on the probability of failure $\widehat{COV_{P_f}}_{AK-MCS}$ is verified to ensure the consistency of the Monte Carlo Simulations. In case the COV is too high, new samples are added to the Monte Carlo population used in AK-MCS and the method goes back to step 7. Otherwise, if the COV is below a user defined threshold the failure probability obtained with the AK-MCS method is the final estimation.

One can note that step 7 of the AK-MCS algorithm involves the resolution of the numerical model. Given the finite element models we consider here (of the form given in Eq. (1)), the idea pursued in the present article is to reduce the numerical cost of this step (and thus the whole reliability analysis) by applying model order reduction method to the resolution of Eq. (1). The obtained approximate solution can thus be used in the AK-MCS algorithm if this approximation reaches a given accuracy threshold. To this purpose, next section introduces the retained reduced basis approach.

3.2. Reduced-Basis Modeling

Model order reduction is a technique for decreasing the computational cost associated to the resolution of a full order model in numerical simulations, i.e. decrease the cost associated with the resolution of the system of Eq. (1). One of the existing model order reduction approaches, which will be considered in this work, is reduced-basis modelling or reduced-order modeling by projection.

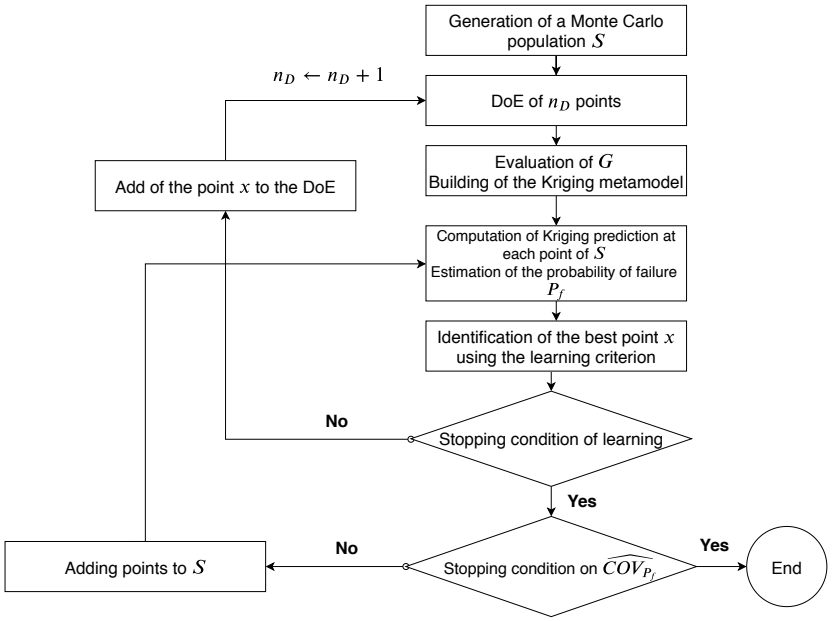

Figure 1: Flowchart of the AK-MCS Algorithm.

This method aims at solving the system of equations (1) by projection onto a reduced basis denoted $\boldsymbol{\Phi} = (\boldsymbol{\Phi}_1, \ldots, \boldsymbol{\Phi}_{n_{RB}})$, where $\boldsymbol{\Phi}_i,\ i = 1, \ldots, n_{RB} \in \mathbb{R}^n$. The initial problem projected on the reduced basis $\boldsymbol{\Phi}$ is then rewritten:

$$\boldsymbol{\Phi}^T \boldsymbol{K}(\boldsymbol{x}) \boldsymbol{\Phi} \boldsymbol{\alpha}(\boldsymbol{x}) = \boldsymbol{\Phi}^T \boldsymbol{F}(\boldsymbol{x}) \tag{12}$$

where $\boldsymbol{\alpha}(\boldsymbol{x}) \in \mathbb{R}^{n_{RB}}$ are the coefficients of the state vector $\boldsymbol{u}(\boldsymbol{x})$ expressed in the reduced basis $\boldsymbol{\Phi}$. Thus the new problem to solve is a linear system of $n_{RB} \ll n$ equations. Indeed the projected problem involves the inversion of the projected stiffness matrix $\boldsymbol{\Phi}^T \boldsymbol{K}(\boldsymbol{x}) \boldsymbol{\Phi} \in \mathbb{R}^{n_{RB} \times n_{RB}}$ and provides after resolution the vector $\boldsymbol{\alpha}(\boldsymbol{x})$. We should note that the projected matrix size is very low compared to the size of the initial stiffness matrix which can reach millions of dof (degrees of freedom) for large-scale finite elements problems. On the other hand, it was found empirically and is generally accepted in the reduced order modelling community [13], that the size of an acceptable reduced basis is in the order of a few dozen for a large variety of engineering problems. The reduced solution is then obtained as $\tilde{\boldsymbol{u}}(\boldsymbol{x}) = \boldsymbol{\Phi} \boldsymbol{\alpha}(\boldsymbol{x})$. In practice, the exact

error between the reduced solution and the real one is not computed (since it would defeat any computational savings). Various error estimation techniques exist such as [16, 38, 39, 40, 41]. In this paper, we first propose the following residual based error estimator [16] (low computational cost) to approximate the accuracy associated to reduced basis solutions :

$$\epsilon_{RB}(\boldsymbol{x}) = \frac{||\boldsymbol{K}(\boldsymbol{x})\boldsymbol{\Phi}\boldsymbol{\alpha}(\boldsymbol{x}) - \boldsymbol{F}(\boldsymbol{x})||_2}{||\boldsymbol{F}(\boldsymbol{x})||_2} \tag{13}$$

So far, the reduced basis $\boldsymbol{\Phi}$, on which the problem is projected, was not specified as many methods exist to define a projection subspace [14, 39, 13], which include very effective methods for affinely parametrized equations. However, the method used here was sought such as to be applicable to all linear problems, including to those for which finding the affine decomposition might be very hard and for which simpler alternatives might be preferable. Thus, in this paper, an on-the-fly method [42], which will be described in details in the next section, is used to construct the reduced basis. Indeed, this method is well suited to the combination with active learning as it consists in enriching the reduced basis iteratively along the sequential reliability estimation procedure with all the simulations for which the full solution of the system Eq. (1) was computed. In practice, both for the construction of the reduced-basis and for the computation of the residual, the stiffness matrix $\boldsymbol{K}(\boldsymbol{x})$ needs in general to be assembled. The computational cost of this operation can be non negligible in general, however, for large-scale problems it becomes increasingly negligible compared with solving the system in Eq. (1). Besides the assembly of the matrix $\boldsymbol{K}(\boldsymbol{x})$, the computation of the residual $\epsilon_{RB}(\boldsymbol{x})$ only involves matrix-vector products and differences whose computational costs are also negligible for problems of large dimensions. Model order reduction is thus a powerful technique to reduce computational cost and its use within the AK-MCS approach is proposed in the following.

4. Proposed Method

4.1. General concept

We propose here an hybrid reliability analysis method coupling active learning approaches and reduced-basis modeling. Indeed, some points of the DoE may not need to be evaluated using the full numerical simulations. Points located close to the limit state might be in the vicinity of other infill points which have previously been computed (using the full order model). Consequently, reduced-order solutions at these points are likely to have good accuracy. The proposed procedure starts with the definition of an initial DoE which at the same time serves to initialize both the surrogate model and the reduced basis. In fact, the first point of the DoE is evaluated with the full numerical model and is considered as the first element of the reduced basis. At each point of the DoE, the response of the reduced-basis model and a criterion on the accuracy of the reduced solution are computed. Then, based on the accuracy criterion, it is decided either to use the reduced solution or to solve the full order model. In this latter case, the solution computed using the full order model is also used to enrich the reduced basis $\mathbf{\Phi}$. A surrogate is then fitted using both reduced and full solutions. At each iteration of the learning phase the same operations are carried out to evaluate the infill points. In the next sections the method combining the algorithm AK-MCS and reduced basis modeling with different criteria is described.

4.2. Coupling of AK-MCS and reduced-basis modeling

We propose here an algorithm combining the method AK-MCS and reduced basis modeling based on the framework presented in the previous sections. It involves to take in consideration reduced solutions in the initialization and learning phases of AK-MCS. The algorithm of the proposed method is provided in Algorithm 1 and described below. The algorithm starts with the initialization of the reduced basis. Therefore, the first sample of the initial DoE is computed and normalized to serve as the first element $\mathbf{\Phi}_1$ of the reduced basis. Then all

other samples of the DoE, i.e. samples of the inital DoE and infill points added in the learning phase, are evaluated according to the following steps:

1. Computation of the reduced solution $\tilde{\boldsymbol{u_i}}$ at the point $\boldsymbol{x}^i$ by projection on the available reduced basis.
2. Computation of the residual $\epsilon_{RB}(\boldsymbol{x}^i)$ for the previous solution based on Eq. (13).
3. Evaluation of the accuracy of the solution $\tilde{u_i}$. If the value of $\epsilon_{RB}(\boldsymbol{x}^i)$ is below a user defined threshold ϵ, the reduced solution is considered to be accurate enough and is added to the DoE. Otherwise, go to next step.
4. If the reduced solution is found not to be accurate enough based on the previous threshold, the full numerical problem is solved. The associated result $\boldsymbol{u_i}$ is added to the DoE and also used to enrich the reduced basis after orthonormalization as shown in Eq. (14) and (15).

$$\boldsymbol{\Phi}_i = \boldsymbol{u_i} - \sum_{k=1}^{i-1} < \boldsymbol{u_i}, \boldsymbol{\Phi}_k > \boldsymbol{\Phi}_k \tag{14}$$

$$\boldsymbol{\Phi}_i = \frac{\boldsymbol{\Phi}_i}{||\boldsymbol{\Phi}_i||_2} \tag{15}$$

with $< \cdot, \cdot >$ the L^2 scalar product.

The proposed method adaptively makes the choice of using reduced-basis solutions or the full numerical model. This coupling can thus greatly reduce the execution time of AK-MCS since the computation of reduced solutions and residuals are less expensive than the resolution of the full finite element problem.

4.3. Coupling of AK-MCS and reduced-basis modeling with preconditioned residuals

While the residuals of Eq. (13) can be used as a first estimation of the accuracy of the reduced basis solution it may be insufficiently accurate in some cases, depending in particular on the conditioning number of the stiffness matrix. Furthermore, it may not be easy to decide on a threshold based on the relative

Algorithm 1: Coupling algorithm

Generate a Monte Carlo population S of size $n_S = n_{MC}$

Define an initial DoE D of n_D samples

$\boldsymbol{u} \leftarrow$ solution of $\boldsymbol{K}(\boldsymbol{x}^1)\boldsymbol{u}(\boldsymbol{x}^1) = \boldsymbol{F}(\boldsymbol{x}^1)$

$y_{doe} \leftarrow G(\boldsymbol{u}, \boldsymbol{x}^1)$

for $\boldsymbol{x} \in D \backslash \{\boldsymbol{x}^1\}$ **do**

  $\boldsymbol{\alpha} \leftarrow$ solution of $\boldsymbol{\Phi}^T\boldsymbol{K}(\boldsymbol{x})\boldsymbol{\Phi}\boldsymbol{\alpha}(\boldsymbol{x}) = \boldsymbol{\Phi}^T\boldsymbol{F}(\boldsymbol{x})$; $\quad G(\boldsymbol{x}) \leftarrow \boldsymbol{\Phi}\alpha$

  $\epsilon_{RB} \leftarrow \frac{||\boldsymbol{K}\boldsymbol{\Phi}\boldsymbol{\alpha}-\boldsymbol{F}||_2}{||\boldsymbol{F}||_2}$

  if $\epsilon_{RB} > \epsilon$ **then**

    $\boldsymbol{u} \leftarrow$ solution of $\boldsymbol{K}(\boldsymbol{x})\boldsymbol{u}(\boldsymbol{x}) = \boldsymbol{F}(\boldsymbol{x})$

    $\boldsymbol{V} \leftarrow \boldsymbol{u} - \boldsymbol{\Phi}(\boldsymbol{\Phi}^T\boldsymbol{u})$; $\quad \boldsymbol{\Phi} \leftarrow [\boldsymbol{\Phi}, \frac{\boldsymbol{V}}{||\boldsymbol{V}||_2}]$

  $y_{doe} \leftarrow [y_{doe}, G(\boldsymbol{u}, \boldsymbol{x})]$

while $COV < 10\%$ **do**

  while *learning stopping criterion not reached* **do**

    Fit Kriging model $\hat{G}$ with (D, y_{doe})

    $\hat{Y}, \sigma_Y \leftarrow \hat{G}(\boldsymbol{x}), \forall \boldsymbol{x} \in S$

    $P_f \leftarrow \frac{n_{\hat{G}\leq 0}}{n_S}$; $\quad COV \leftarrow \sqrt{\frac{1-P_f}{P_f \cdot n_S}}$

    $U_{learning} \leftarrow \frac{|\hat{Y}|}{\sigma_Y}$

    $\boldsymbol{x} \leftarrow \underset{\boldsymbol{x'} \in S}{\arg\min}\ U_{learning}(\boldsymbol{x'})$

    if $U_{learning}(\boldsymbol{x}) < 2$ **then**

      $\boldsymbol{\alpha}(\boldsymbol{x}) \leftarrow$ solution of $\boldsymbol{\Phi}^T\boldsymbol{K}(\boldsymbol{x})\boldsymbol{\Phi}\boldsymbol{\alpha}(\boldsymbol{x}) = \boldsymbol{\Phi}^T\boldsymbol{F}(\boldsymbol{x})$; $\quad \boldsymbol{u} \leftarrow \boldsymbol{\Phi}\boldsymbol{\alpha}$

      $\epsilon_{RB} \leftarrow \frac{||\boldsymbol{K}\boldsymbol{\Phi}\boldsymbol{\alpha}-\boldsymbol{F}||_2}{||\boldsymbol{F}||_2}$

      if $\epsilon_{RB} > \epsilon$ **then**

        $\boldsymbol{u} \leftarrow$ solution of $\boldsymbol{K}(\boldsymbol{x})\boldsymbol{u}(\boldsymbol{x}) = \boldsymbol{F}(\boldsymbol{x})$

        $\boldsymbol{V} \leftarrow \boldsymbol{u} - \boldsymbol{\Phi}(\boldsymbol{\Phi}^T\boldsymbol{u})$; $\quad \boldsymbol{\Phi} \leftarrow [\boldsymbol{\Phi}, \frac{\boldsymbol{V}}{||\boldsymbol{V}||_2}]$

      $D \leftarrow [D, \boldsymbol{x}]$; $\quad y_{doe} \leftarrow [y_{doe}, G(\boldsymbol{u}, \boldsymbol{x})]$

    else

      learning stopping criterion reached

  Generate a Monte Carlo population S^* of size n_{MC}

  $S \leftarrow [S, S^*]$

End of algorithm

residual of Eq. (13) which is defined on the loading vector, as one is more interested in the relative error on the state variable vector (e.g. displacement or temperature vector). The use of a preconditioner $\boldsymbol{P}$ can thus improve the error estimators based on the residuals [43] as the preconditioned residual is homogeneous to the state variable. Thus, the following preconditioned residual is also considered in this section:

$$\epsilon_{RB}^{P}(\boldsymbol{x}) = \frac{||\boldsymbol{P}^{-1}\boldsymbol{K}(\boldsymbol{x})\boldsymbol{\Phi}\boldsymbol{\alpha}(\boldsymbol{x}) - \boldsymbol{P}^{-1}\boldsymbol{F}(\boldsymbol{x})||_2}{||\boldsymbol{P}^{-1}\boldsymbol{F}(\boldsymbol{x})||_2} \tag{16}$$

The computation of the preconditioned residual $\epsilon_{RB}^{P}(\boldsymbol{x})$ is in general more expensive than the computation of $\epsilon_{RB}(\boldsymbol{x})$ due to the computation of the term $\boldsymbol{P}^{-1}\boldsymbol{K}(\boldsymbol{x})\boldsymbol{\Phi}\boldsymbol{\alpha}(\boldsymbol{x})$. However for preconditioners that are independent of the parameter $\boldsymbol{x}$, the decomposition of $\boldsymbol{P}$ can be stored once for all. Thus the only cost is the resolution of the system according to the type of factorization chosen, which has to be done in any case, and which thus does not induces any significant additional computational cost. Hence the previously proposed method for coupling AK-MCS and reduced basis modeling can be improved by using the preconditioned residual $\epsilon_{RB}^{P}(\boldsymbol{x})$. This new estimates improves the residual based error estimation used to decide if the reduced solution is accurate enough to be used in place of the full numerical solution.

There exist several ways of constructing a preconditioner. In this paper, the proposed method will be run with two possible preconditioner construction techniques:

- the mean point preconditioner [44]: the full numerical model is computed at the mean point of the physical design space and the resulting matrix $\boldsymbol{K}^0$ serves as preconditioner $\boldsymbol{P} = \boldsymbol{K}^0$.

- the nearest point preconditioner: every time the full numerical model is computed to enrich the reduced basis, the matrix $\boldsymbol{K}^i = \boldsymbol{K}(\boldsymbol{x}^i)$ is stored to serve as a possible preconditioner (let us denote $\mathcal{X}_{full} = \{\boldsymbol{x}^i,\ i = 1, \ldots, n_{full}\} \subset S$ which contains the point where the full solution has been computed). Then, for each sample evaluation, at point $\boldsymbol{x}^* \notin S$, the preconditioned

residual is computed using $\boldsymbol{P} = \boldsymbol{K}^i$ where $\boldsymbol{x}^i = \min_{\boldsymbol{x} \in \mathcal{X}_{full}} ||\boldsymbol{x} - \boldsymbol{x}^*||_2$.

Note that the preconditioning of the residual also makes it easier to set the value of the threshold ϵ in the proposed algorithm. Indeed based on error bound provided in [45], for a good choice of preconditioner, $\epsilon_{RB}^P(\boldsymbol{x})$ can be seen as a good approximation of the relative error of the reduced basis solution $\tilde{\boldsymbol{u}}(\boldsymbol{x})$ compared to the true solution $\boldsymbol{u}(\boldsymbol{x})$. It can be expected that if ϵ is set to have a low relative error on $\boldsymbol{u}(\boldsymbol{x})$ (e.g. 10^{-3}), the error on $G(\boldsymbol{x})$ will also be low. This is generally the case, as G is usually only mildly nonlinear in $\boldsymbol{u}(\boldsymbol{x})$. However, it is certainly dependent on the form of $G : \boldsymbol{x} \to G(\boldsymbol{u}(\boldsymbol{x}), \boldsymbol{x})$ and in case $G(\boldsymbol{x})$ is highly nonlinear in $\boldsymbol{u}(\boldsymbol{x})$ the choice of ϵ may need more than one trial to obtain a reasonable value.

4.4. Potential extensions to multi-fidelity modeling with co-kriging

The use of both reduced and complete solutions as solutions of the same model to fit a surrogate model can be discussed. In fact, the data has different fidelity levels: the complete solutions are high-fidelity data and the reduced solutions are low-fidelity data with n_F different levels. Indeed, each time the reduced basis is enriched the reduced model is improved and corresponds to a new level of fidelity. The use of a surrogate model based on multiple fidelity levels such as a co-kriging could thus be considered. However, only relatively few simulations are available for each fidelity level, which makes it next to impossible to construct a co-kriging model based on n_F fidelity levels. An approximation would be to simplify the problem as having only two fidelities and use a two-fidelity co-kriging model. This reformulation as a co-kriging problem using the solution obtained with the full numerical model as high fidelity data and the one obtained with the reduced basis model as low-fidelity data can be investigated in three different ways:

1. by trying to replace Kriging by co-Kriging all along the learning algorithm,
2. by using Kriging in the learning and replacing the final Kriging by a co-Kriging with the low and high-fidelity training points,

3. same strategy than the second one, except that here the low-fidelity points are recomputed at the end using the final reduced basis in order to have the same low-fidelity level.

Their comparison will be illustrated in Appendix A.

The two proposed strategies coupling AK-MCS and reduced-basis modeling with or without the use of a preconditioner are numerically investigated to compare their performances on two applications in the next section. The first one concerns a thermal problem and the second one a mechanical problem.

5. Applications

In the following, the two numerical applications are presented. For each one a description of the physical problem is given, followed by the numerical comparisons between the different strategies to estimate the probability of failure.

5.1. First application example: Reliability analysis on a thermal problem

5.1.1. Description of the problem

In this section, the application considered is a reliability analysis, which involves the heat transfer through the combustion chamber wall of a regeneratively cooled rocket engine [46, 47, 16]. In such an engine, liquid hydrogen (LH2) flowing through cooling channels in the combustion chamber wall at a temperature of 40K is used for cooling the engine. We consider that failure occurs when the maximum temperature of the inner wall of the combustion chamber exceeds a critical value T_{allow}, which corresponds to the cooling channel walls rupture, due to thermally induced stresses.

A schematic of the combustion chamber of a typical regeneratively cooled liquid hydrogen (LH2) liquid oxygen (LOX) rocket engine is shown on Fig. 2. As illustrated on this figure, two different parts made of two different materials form the combustion chamber wall: an internal side made of a copper alloy and an external jacket made of a Ni alloy. Heat exchanges may happen through

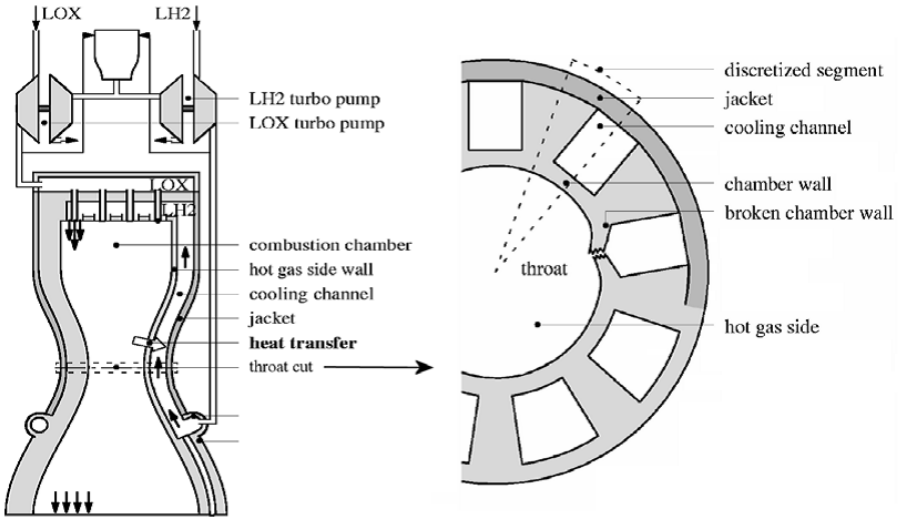

Figure 2: Schematic of a regeneratively cooled rocket engine combustion chamber.

convection between the combustion chamber wall and the sources of heat (combustion chamber gases) and cooling (liquid hydrogen) and also with the exterior. Considering these boundary conditions, the resulting thermal transfer depends on the following parameters: the conductivity of the inner side of the wall (k_{Cu}), the conductivity of the jacket (k_{Ni}), the temperature of the gases on the inner side of the combustion chamber (T_{hot}), the film convection coefficient on the inner side of the combustion chamber (h_{hot}), the temperature on the outer side of the combustion chamber (T_{out}), the film convection coefficient on the outer side of the combustion chamber (h_{out}), the temperature of the cooling fluid (T_{cool}) and the film convection coefficient on the cooling channel side (h_{cool}). These parameters and the maximum temperature allowable T_{allow} are supposed to be uncertain and are modeled by independent random variables following probability distributions given in Table 1. Thermal field at stationary equilibrium is obtained by resolution of a convection-diffusion equation by a finite element approach. The finite element mesh of the combustion chamber wall and the boundary conditions are illustrated in Fig. 3.

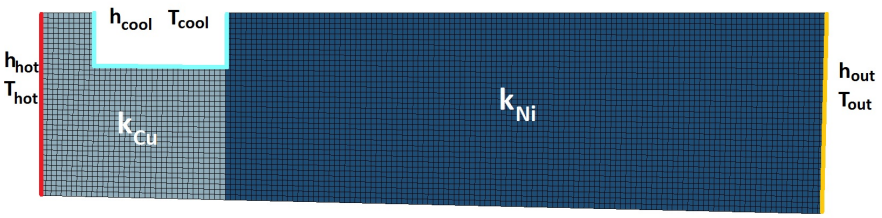

Figure 3: Finite element mesh of the combustion chamber wall and the boundary conditions of the thermal problem.

Input	k_{Cu}	k_{Ni}	T_{hot}	h_{hot}	T_{out}	h_{out}	T_{cool}	h_{cool}	T_{allow}
Unit	W/mK	W/mK	K	kW/m^2K	K	kW/m^2K	K	kW/m^2K	K
Probability law	Gaussian	Gaussian	Uniform	Uniform	Uniform	Uniform	Uniform	Uniform	Uniform
Mean	310	75	900	31	293	6	40	250	230
COV	2%	2%							
Half-range			10%	10%	5%	5%	5%	10%	7.5%

Table 1: Probability distributions of the thermal problem parameters.

Here an in-house finite element solver coded in Python is used to compute the thermal field. Thus we have access to the maximum temperature and we can deduce the performance function, defined here as $G(\boldsymbol{x}) = T_{allow}(\boldsymbol{x}) - T_{max}(\boldsymbol{x})$. Then the failure probability can be estimated using Monte Carlo sampling or using AK-MCS based strategies. The results of these comparisons are presented in the following.

5.1.2. Results

First, a Monte Carlo Simulation was run to have an accurate estimation of the failure probability used as reference in the following comparison. The

estimation obtained with standard Monte Carlo was $\hat{P}_{f_{MC}} = 6.22 \cdot 10^{-3}$ with an estimated COV of 5.65% (for $n_{MC} = 5 \times 10^4$). The AK-MCS method was implemented using the reduced-basis coupling with the classical and the mean point preconditioned residual criteria. These two methods were run on the same thermal problem described in the previous section. In order to verify the residual is a valid coupling criterion, the Pearson correlation coefficient between the residual and the *real error* is estimated (*real error* is defined as the error between the reduced solution and the finite element solution). These estimations are done for different reduced basis sizes and are computed using the residuals and real error values on a random Monte Carlo population.

As depicted on Fig. 4, the preconditioned residual is almost perfectly correlated to the real error, which can be explained by the well-posedness of the problem. The correlation between the real error and the non preconditioned residual has a lower score, in particular for larger sizes of the reduced basis.

The graphical representation of the first three modes of a temperature reduced basis constructed on-the-fly during a run of the coupling based on ϵ_{RB} for $\epsilon = 10^{-3}$ is given in Fig. 5. The construction methodology used implies that the first mode is the dominant mode, meaning that it is the one that represents the best the typical thermal fields. However, to capture finer variations of the thermal field and thus achieve accurate reduced solutions, additional basis vectors (corresponding to additional modes) are needed. Therefore it is interesting to study the influence of the value ϵ taken as threshold for the coupling criterion on the proposed method's performances. To this end, the following procedure is carried out:

- Run AK-MCS algorithm and save the resulting DoE (i.e. initial DoE and infill points)
- For varying threshold ϵ, apply the reduced basis coupling on the samples of the AK-MCS DoE in the same order they were added by AK-MCS algorithm.

Here two criteria are used to compare the proposed method's performances for

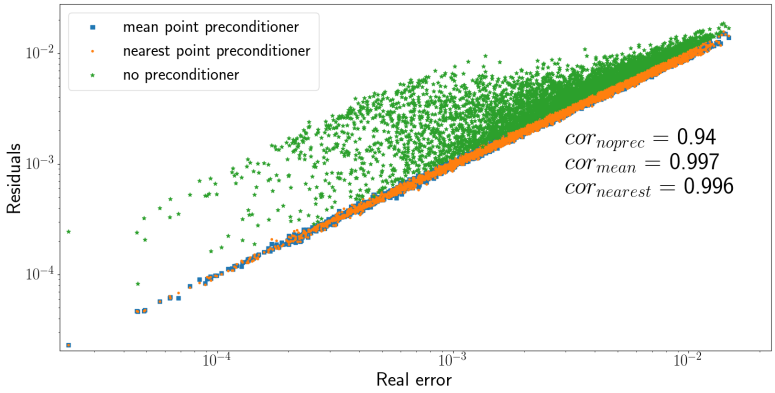

Reduced basis size = 5

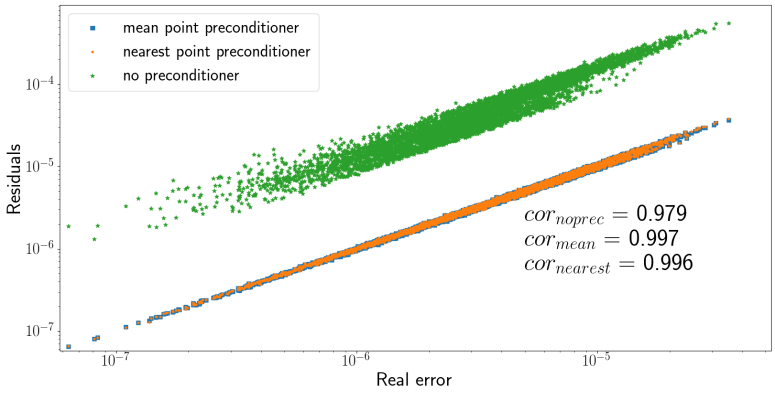

Reduced basis size = 10

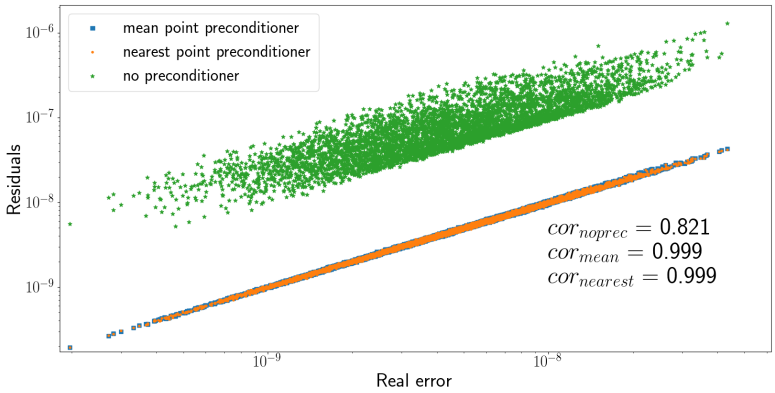

Reduced basis size = 20

Figure 4: Correlation between the residuals and the real error for the thermal problem. Three reduced basis sizes (5, 10 and 20) are considered.

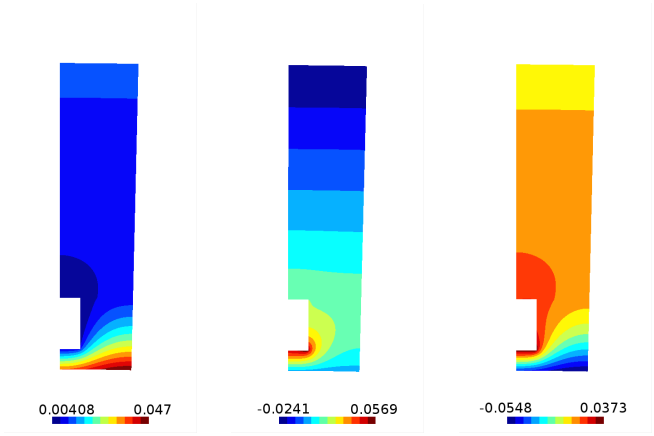

Figure 5: First three temperature modes obtained using the on-the-fly constructing procedure through AK-MCS for the thermal problem.

different ϵ:

- the speed up achieved by using the proposed method over AK-MCS, i.e. the ratio of number of evaluations of the full numerical model in AK-MCS to the number of its evaluations when using the coupling. Note that we only compare the ratios of the full numerical models, as the cost of inverting the reduced basis model becomes negligible as the size (number of degrees of freedom) of the problem increases.

- the relative accuracy of the failure probability estimation. Here we compare the estimations of $\widehat{P_f}_{AK-MCS+RB}$ and $\widehat{P_f}_{AK-MCS}$ on the same initial DoE and Monte Carlo population. The relative accuracy is thus defined by the formula $1 - \frac{|\widehat{P_f}_{AK-MCS} - \widehat{P_f}_{AK-MCS+RB}|}{\widehat{P_f}_{AK-MCS}}$ where a perfect accuracy will have a value equal to 1.

In order to take into account the stochastic variation of the AK-MCS approach in the assessment of the influence of the parameter ϵ, the previous procedure was run 10 times for different initial DoEs and Monte Carlo populations. The mean of the two criteria described just above were thus computed for different values

of the threshold. Their evolution is given on Fig. 6 for the non preconditioned residual ϵ_{RB} and on Fig. 7 and Fig. 8 for the preconditioned residuals ϵ^P_{RB}.

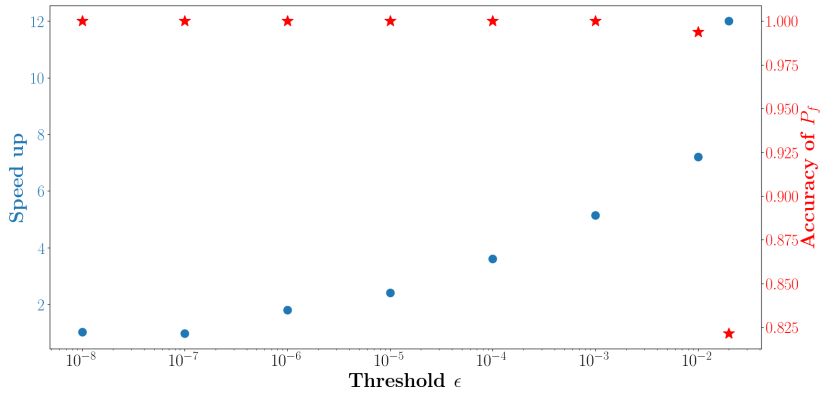

Figure 6: Accuracy (red stars) of P_f and speed up (blue dots) of the proposed method as a function of the threshold ϵ on the non preconditioned residual for different constant DoEs and Monte Carlo generated by AK-MCS algorithm for the thermal problem.

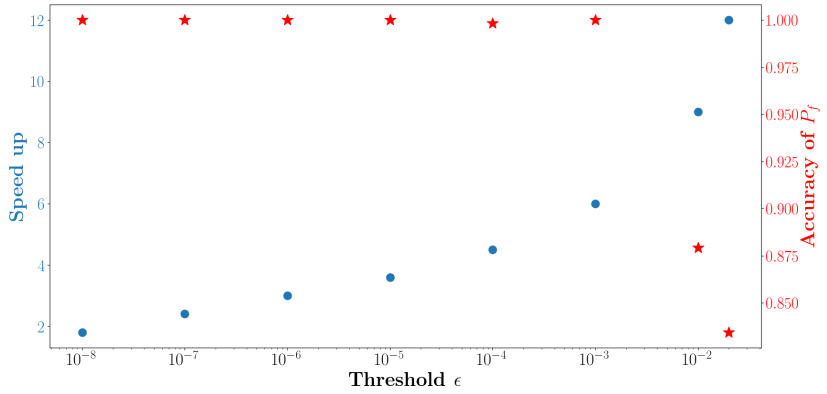

Figure 7: Accuracy (red stars) of P_f and speed up (blue dots) of the proposed method as a function of the threshold ϵ on the preconditioned residuals with the mean point preconditioner for different constant DoEs and Monte Carlo generated by AK-MCS algorithm for the thermal problem.

From these figures a good compromise between speed up obtained by the

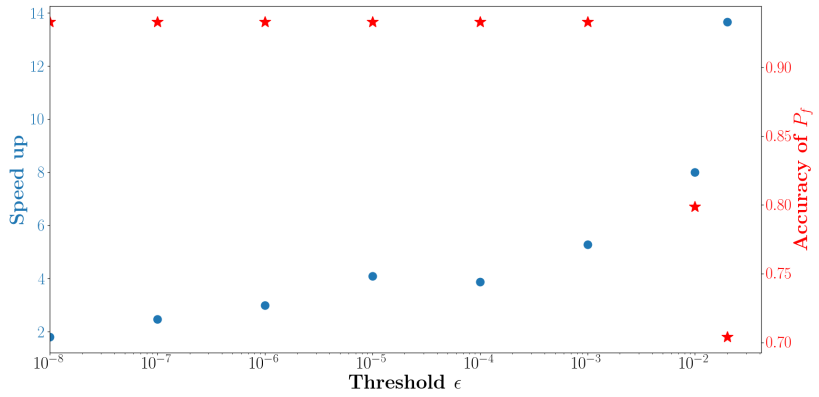

Figure 8: Accuracy (red stars) of P_f and speed up (blue dots) of the proposed method as a function of the threshold ϵ on the preconditioned residuals with the nearest point preconditioner for different constant DoEs and Monte Carlo generated by AK-MCS algorithm for the thermal problem.

proposed algorithm and accuracy of the probability of failure estimate results seems to be reached for $\epsilon = 10^{-3}$. It can also be noted that even if the correlation of the real error with the non preconditioned residual is not as good as if preconditioning is used (as shown by Fig. 4), it is sufficient here to obtain satisfying results in terms of estimating the probability of failure. On the basis of these results, AK-MCS and the proposed methods are now compared in more details for $\epsilon = 10^{-3}$. Compared to the previous study, one should note that, in the proposed approach, the selection of enrichment points is now potentially led by the solution obtained using the reduced basis approximation. For each version of the proposed methods (with and without preconditioning) 30 computations of both the proposed method and AK-MCS for a same initial DoE and Monte Carlo population have been run. The sample mean $\overline{P_f}$ and corrected sample standard deviation $\overline{\sigma_{P_f}}$ based on the results of these runs can be found on Table 2 and Table 3.

First of all, note that the sample means obtained for the AK-MCS algorithm and for the proposed method are consistent with the Monte-Carlo refer-

	$\overline{P_f}$	$\overline{\sigma_{P_f}}$	n_{sim}	n_{full}
MCS	6.22×10^{-3}	3.5×10^{-4}	5×10^4	5×10^4
AK-MCS	6.52×10^{-3}	1.88×10^{-4}	38.2	38.2
AK-MCS + RB	6.52×10^{-3}	1.90×10^{-4}	38.1	6.7

Table 2: Results of MCS and mean results of AK-MCS and AK-MCS + RB with no preconditioned residual for the thermal problem.

	$\overline{P_f}$	$\overline{\sigma_{P_f}}$	n_{sim}	n_{full}
MCS	6.22×10^{-3}	3.5×10^{-4}	5×10^4	5×10^4
AK-MCS	6.52×10^{-3}	1.88×10^{-4}	38.2	38.2
AK-MCS + RB	6.52×10^{-3}	1.88×10^{-4}	40.7	6

Table 3: Results of MCS and mean results of AK-MCS and AK-MCS + RB with the mean point preconditioner for the thermal problem.

	$\overline{P_f}$	$\overline{\sigma_{P_f}}$	n_{sim}	n_{full}
MCS	6.22×10^{-3}	3.5×10^{-4}	5×10^4	5×10^4
AK-MCS	6.47×10^{-3}	3.03×10^{-4}	38.1	38.1
AK-MCS + RB	6.47×10^{-3}	3.02×10^{-4}	39.4	6

Table 4: Results of MCS and mean results of AK-MCS and AK-MCS + RB with the nearest point preconditioner for the thermal problem.

ence $\hat{P}_{f_{MC}} = 6.22 \cdot 10^{-3}$ (with an estimated COV of 5.65%). More precisely, the sample mean obtained for both proposed method variants are very close to the AK-MCS reference $\widehat{P_f}_{AK-MCS}$ sample mean. Note as well that the values of the estimated variances don't take extreme values when the reduced basis is used and are even very close to the reference $\widehat{\sigma}_{\widehat{P_f}_{AK-MCS}}$, especially for the preconditioned residual strategy. For these computations the speed up of the algorithm in terms of full numerical simulations for the preconditioned residual strategy is of 6.37 and 6.33 respectively for the mean point and the nearest

point preconditioner. For the non preconditioned residual strategy the speed up factor is 5.74. Moreover, for a run of the coupling algorithm with the mean point and the nearest point preconditioners full evaluations represent on average respectively 15% and 15.5% of the total number of evaluations. Without preconditioning the percentage of full evaluations is on average 17.8%.

Moreover, the different reformulations of the problem with co-Kriging (cf. section 4.4) have been tested on this application. Detailed results are given in Appendix A. The only strategy that worked well was the third one, that consists in using Kriging in the learning phase, then recomputing all low-fidelity points with the final reduced basis and finally constructing a co-kriging using these low-fidelity data and the high-fidelity data. However, the use of co-Kriging does not improve significantly the accuracy of the estimation for this problem, whereas it slightly increases the computational cost, as all reduced basis solutions must be reevaluated. Therefore, we chose to keep the results obtained with the kriging surrogate model in this study.

To confirm the promising results obtained with the proposed approaches on this first application example, a second, more complex application is investigated in the following.

5.2. Second application example: failure of a composite laminate plate with a hole under complex loading

5.2.1. Description of the problem

We now consider the application of the proposed methods on a mechanical problem involving a potentially non-symmetric laminates, due to uncertainties in the ply layup. The test case illustrated on Fig. 9 is the reliability analysis of a one-side clamped laminated plate with a hole under uniform vertical pressure and in-plane shear loading on the side opposite to the clamping considering the Tsaï-Hill failure criterion recalled below:

$$\left(\frac{\sigma_L(\boldsymbol{\theta},\boldsymbol{h})}{X_{ult}}\right)^2+\left(\frac{\sigma_T(\boldsymbol{\theta},\boldsymbol{h})}{Y_{ult}}\right)^2+\left(\frac{\tau_{LT}(\boldsymbol{\theta},\boldsymbol{h})}{\tau_{ult}}\right)^2-\frac{\sigma_L(\boldsymbol{\theta},\boldsymbol{h})\sigma_T(\boldsymbol{\theta},\boldsymbol{h})}{X_{ult}^2}>1 \quad (17)$$

where X_{ult}, Y_{ult} and τ_{ult} are the ultimate strengths and σ_L, σ_T and τ_{LT} are respectively the longitudinal, transverse and shear stresses. The variables $\boldsymbol{\theta}$ and

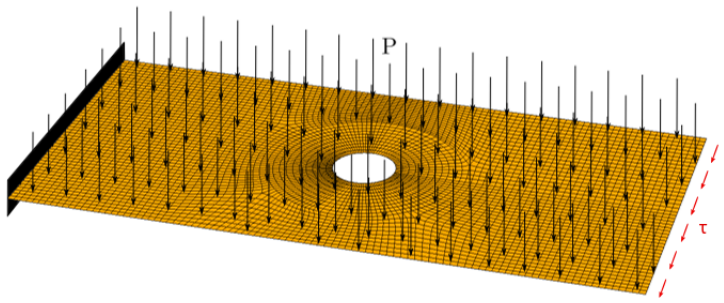

Figure 9: Boundary conditions and loading on the laminated plate.

$\boldsymbol{h}$ are respectively the fiber orientation angles and the ply thickness for each of the six plies of the laminate. It is assumed that, due to manufacturing uncertainties, these parameters are random and thus are modeled by the following independent random variables:

- the ply thicknesses h_i follow gamma distributions $\Gamma(\mu, \sigma, \gamma)$ with parameters provided in Table 5,
- the fiber orientation angles θ_i follow uniform distributions $\mathcal{U}(a, b)$ with parameters provided in Table 6.

μ	$2 \cdot 10^{-4}$
σ	$2 \cdot 10^{-5}$
γ	0

Table 5: Parameters of the gamma probability distribution used to model all ply thicknesses.

Note that the nominal laminate is thus assumed to have a ply thickness of 0.2 mm and a layup of $[0, 45, -45]_s$. However due to uncertainties, the actual laminate may have different values, in particular it is non-symmetric in general.

	θ_1	θ_2	θ_3	θ_4	θ_5	θ_6
a	-2.5	42.5	-47.5	-47.5	42.5	-2.5
b	2.5	47.5	-42.5	-42.5	47.5	2.5

Table 6: Parameters of the uniform probability distributions used to model the fiber orientation angles.

A MATLAB-based in-house finite element solver is used here to compute the stress field. We used a four-node Mindlin shell element with five degrees of freedom per node with a shear correction factor computed according to [48]. The finite element mesh of the laminate used here is illustrated in Fig. 10. The elastic constants of a ply are provided in Table 7. The longitudinal ultimate tensile and compression strengths (resp. X^T_{ult} and X^C_{ult}), transversal ultimate tensile and compression strengths (resp. Y^T_{ult} and Y^C_{ult}) and ultimate in-plane shear strength (τ_{ult}) of the ply are provided in Table 8.

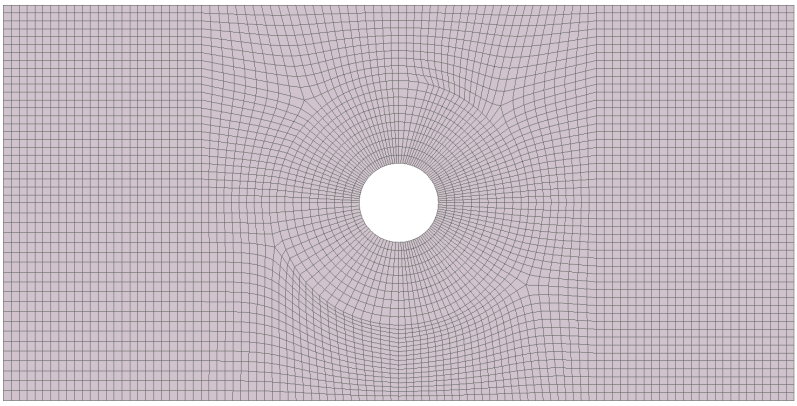

Figure 10: Finite element mesh of the laminated plate with a hole.

In the next section, the failure probability will be estimated using AK-MCS and reliability analysis based on the proposed strategy in order to test the

E_1	E_2	ν_{12}	G_{12}
181 GPa	10.3 GPa	0.28	7.17 GPa

Table 7: Ply elastic constants.

X^T_{ult}	X^C_{ult}	Y^T_{ult}	Y^C_{ult}	τ_{ult}
997 MPa	847 MPa	38 MPa	198 MPa	60 MPa

Table 8: Ply ultimate stresses.

performances of the coupling on the presented problem.

5.2.2. Results

First, a Monte Carlo Simulation was run to have an accurate estimation of the failure probability of this problem. The estimation obtained with standard Monte Carlo was $\hat{P}_{f_{MC}} = 7.6 \times 10^{-4}$ with an estimated COV of 9.36% (for $n_{MC} = 1.5 \times 10^5$).

Then, a similar study as the one for the thermal problem was carried on this problem. First the correlation between the residuals and the real error was estimated. Figure 11 presents the results obtained for different reduced basis dimensions. It can be seen on this figure that the coefficient of correlation between the non preconditioned residual and the real error is very low and that many residuals take values greater than 1 regardless of the size of the reduced basis. This is probably due to the higher ill-conditioning of this problem, compared to the previous one, in particular due to the non symmetric laminates that are considered, inducing bending-shear coupling. On the basis on these results, it would be quite hard to find an efficient threshold ϵ and ensure the effectiveness of the coupling.

The correlation with preconditioned residuals was considered next and is also presented on Fig. 11. Given the higher numerical complexity of this application, both preconditioners presented in Section 4.3 were tested. It can be noted that

the two proposed preconditioners have similar performances for this problem with coefficients of correlation higher than 0.9 which is a significant improvement compared to non preconditioned residual.

As in the thermal problem, the first modes of the displacement field constructed on-the-fly during a run of the coupling, based on ϵ_{RB}^{P} for $\epsilon = 10^{-3}$, can be graphically represented. The representations of the four first basis vectors of the displacement field in the out of plane direction are given in Fig. 12. The first mode has obviously much similarity with the general shape of the displacement field, which again is asymmetric, due to the non-symmetric laminates and induced bending shear coupling. For this same reason, the higher modes represented describe even more complex variations of the displacement fields. Hence, due to this relatively complex behaviour it can be expected that more modes will be required on this application to satisfy the error criterion $\epsilon = 10^{-3}$.

The performance of the proposed methods for different thresholds on ϵ_{RB}^{P} was studied next, following the same process as for the first application, i.e. using the coupling strategy on a fixed DoE generated during a run of AK-MCS for varying thresholds. The mean values of the speed up and accuracy computed over 10 runs as a function of ϵ are given on Fig. 13 for the mean point preconditioner and on Fig. 14 for the nearest point preconditioner.

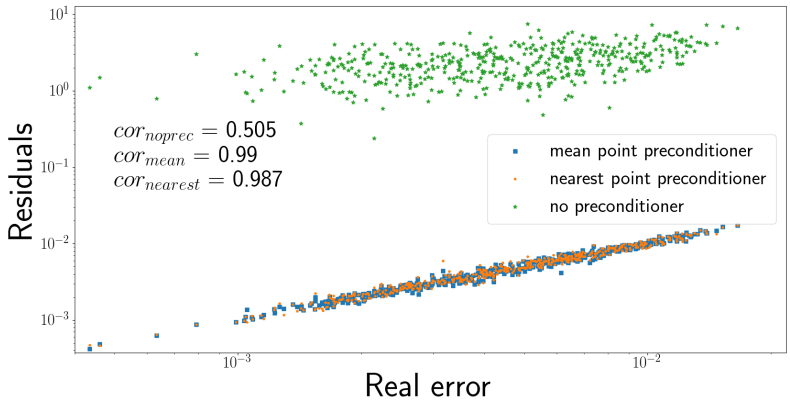

Reduced basis size = 5

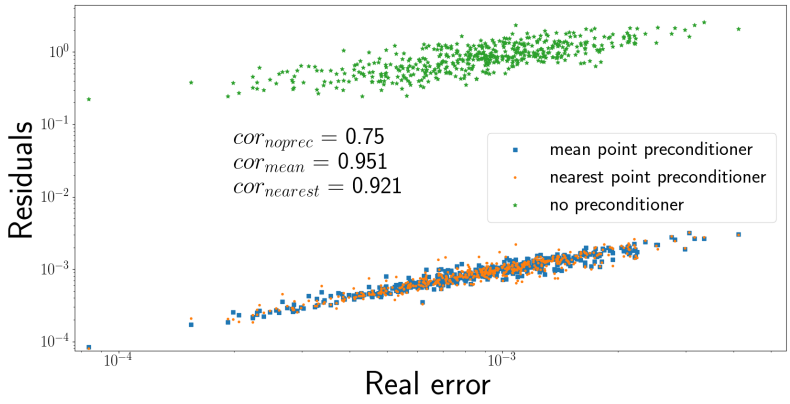

Reduced basis size = 10

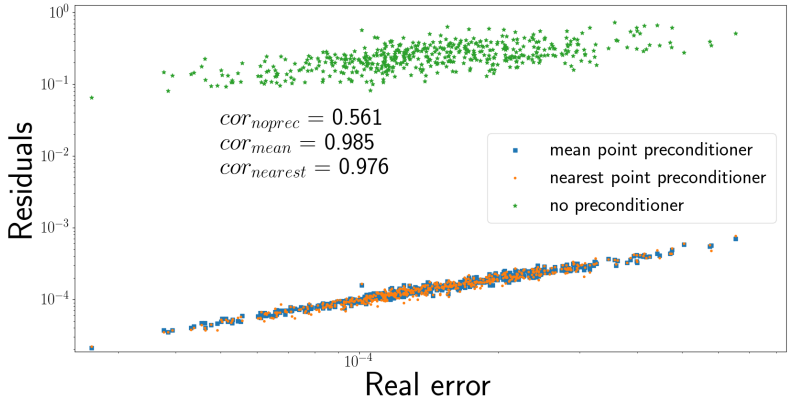

Reduced basis size = 20

Figure 11: Correlation between the residuals and the real error for the laminated plate with a hole problem. Three reduced basis sizes (5, 10 and 20) are considered.

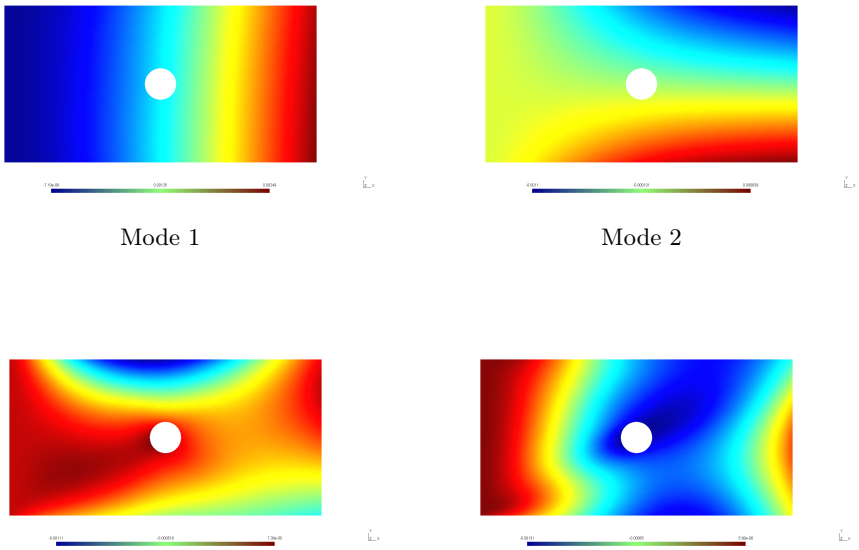

Mode 1 Mode 2

Mode 3 Mode 4

Figure 12: First four Z-displacement modes obtained using the on-the-fly constructing procedure through AK-MCS for the laminated plate with a hole problem.

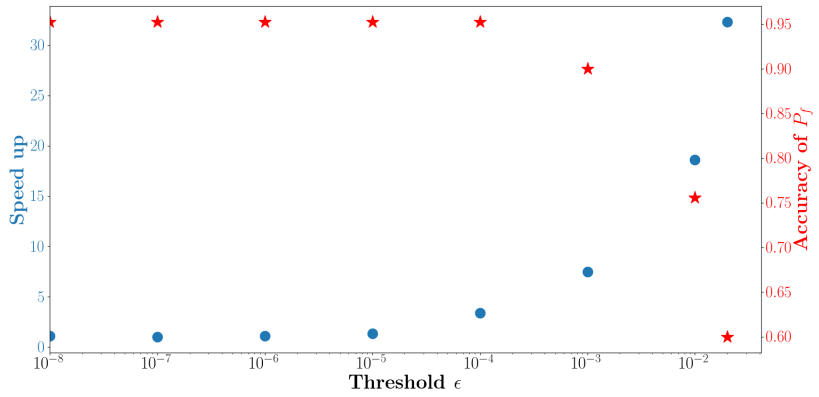

Figure 13: Accuracy (red stars) of the failure probability P_f and speed up (blue dots) as a function of the threshold ϵ on the preconditioned residuals with the mean point preconditioner for different constant DoEs and Monte Carlo generated by AK-MCS algorithm for the laminated plate with a hole problem.

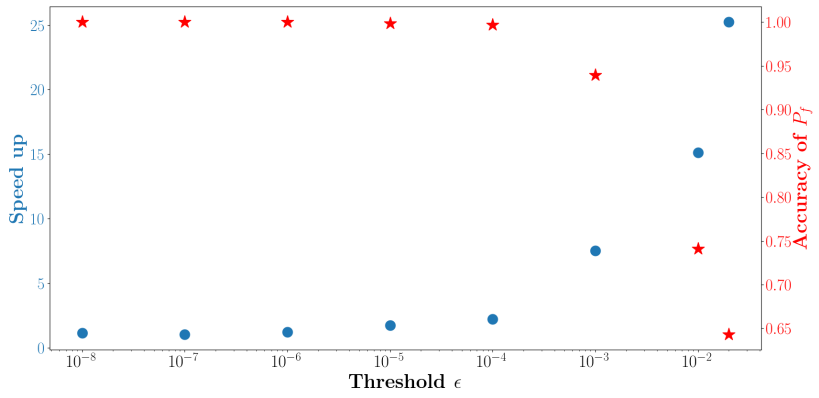

Figure 14: Accuracy (red stars) of the failure probability P_f and speed up (blue dots) as a function of the threshold ϵ on the preconditioned residuals with the nearest point preconditioner for different constant DoEs and Monte Carlo generated by AK-MCS algorithm for the laminated plate with a hole problem.

According to Fig. 13 and Fig. 14 the best compromise between accurate estimations and a consequent acceleration of the reliability analysis method lies

again at $\epsilon = 10^{-3}$ for both preconditioners. Note that this is in-line with our earlier comment that the threshold epsilon can be selected based on a relative value that is considered acceptable on the norm of error in the displacement field. A value of 10^{-3} or 0.1% for the norm of the displacement field relative error seems a sensible value to choose as a start for many problems.

Then AK-MCS and the proposed method were run 40 times for different initial DoEs and Monte Carlo populations with $\epsilon = 10^{-3}$. The resulting sample means $\overline{P_f}$ and corrected sample standard deviation $\overline{\sigma_{P_f}}$ are given in Table 10 for the mean point preconditioner and in Table 9 for the nearest point preconditioner. The mean failure probability estimated by the proposed method is in the 95% confidence interval of the mean results of AK-MCS $[8.20\times10^{-4}, 8.80\times10^{-4}]$. Moreover the corrected sample standard deviations are in the same order of magnitude whether reduced basis solutions are used or not. On average, the use of the proposed methods over AK-MCS allows a speed-up of 6.8 and 6.7 respectively for the mean point and the nearest point preconditioner. Furthermore, for a run of the coupling algorithm the mean point and the nearest point preconditioners full evaluations represent on average respectively only 16.2% and 14.4% of the total number of evaluations.

	$\overline{P_f}$	$\overline{\sigma_{P_f}}$	n_{sim}	n_{full}
MCS	7.6×10^{-4}	7.1×10^{-5}	1.5×10^{5}	1.5×10^{5}
AK-MCS	8.50×10^{-4}	6.36×10^{-5}	100.2	100.2
AK-MCS + RB	8.23×10^{-4}	6.47×10^{-5}	105.7	14.97

Table 9: MCS results and mean results of AK-MCS and AK-MCS + RB with the nearest point preconditioner for the laminated plate with a hole problem.

	$\overline{P_f}$	$\overline{\sigma_{P_f}}$	n_{sim}	n_{full}
MCS	7.6×10^{-4}	7.1×10^{-5}	1.5×10^5	1.5×10^5
AK-MCS	8.47×10^{-4}	5.58×10^{-5}	99.95	99.95
AK-MCS + RB	8.48×10^{-4}	7.14×10^{-5}	98.87	15.97

Table 10: MCS results and mean results of AK-MCS and AK-MCS + RB with the mean point preconditioner for the laminated plate with a hole problem.

5.3. Computational costs for large-scale applications

The previous numerical investigations have been carried out in order to study the performances of the coupling with reduced basis in terms of results accuracy and full solution number reduction. In order to be able to compare to the true probabilities of failure obtained by crude Monte Carlo simulation we considered relatively few degrees of freedom in both the thermal and the mechanical problems. However, the CPU time savings enabled by the use of reduced solutions are particularly interesting for high dimensional problems (large number of degrees of freedom). Hence, we now use refined meshes to compare the CPU times of the coupling with the mean point preconditioner and the classical methods on the two previous problems.

5.3.1. First application example: Reliability analysis on a thermal problem

As the thermal problem admits a simple affine decomposition of the matrix $K(x) = \sum_i \gamma_i(x) K_i$, the assembly of the matrices K_i is done once for all. The reported assembly and system resolutions CPU time corresponds to the assembly made by the computational code *Code Aster* [49]. The CPU time reported in Table 11 corresponds to a problem of 1,321,537 degrees of freedom.

Hence, the speed up in terms of CPU time is about 5 for this problem.

5.3.2. Second application example: failure of a composite laminate plate with a hole under complex loading

For this application, the stiffness matrix $\boldsymbol{K}(\boldsymbol{x})$ has to be assembled for each point x evaluated during the learning procedure. Moreover the force vector $\boldsymbol{F}(\boldsymbol{x})$

	AK-MCS + RB	AK-MCS
assembly time of $\boldsymbol{K}_i$ (once for all)	3.20	3.20
number of evaluations of $G(\boldsymbol{x})$	40	38
number of reduced solutions $\tilde{\boldsymbol{u}}(\boldsymbol{x})$ evaluations	40	38
number of full solutions $\boldsymbol{u}(\boldsymbol{x})$ evaluations	6	38
time of the projection $\boldsymbol{\Phi}^T\boldsymbol{K}_i\boldsymbol{\Phi}$ with the initial reduced basis	0.6	-
time of the projection $\boldsymbol{\Phi}^T\boldsymbol{K}_i\boldsymbol{\Phi}$ with the final reduced basis	1.8	-
mean time of full solution $\boldsymbol{u}(\boldsymbol{x})$ evaluation	43.6	43.6
mean time of reduced solution $\tilde{\boldsymbol{u}}(\boldsymbol{x})$ evaluation	0.01	-
mean time preconditionned residual $\epsilon^P_{RB}(\boldsymbol{x})$ evaluation	1.3	-
total CPU time	324	1657

Table 11: Operations CPU time (in seconds) for the reliability analysis for the thermal problem.

actually does not depend on $\boldsymbol{x}$ here. Thus the value $\boldsymbol{P^{-1}F}$ can be computed once for all at the beginning of the algorithm. The CPU time reported in Table 12 corresponds to a problem of 1,029,700 degrees of freedom. Hence, the speed up in terms of CPU time is about 5.4 for this problem.

6. Conclusions

The present article proposes strategies to improve the efficiency of adaptive sampling surrogate based reliability analysis techniques based on the use of reduced basis solutions over expensive full numerical solutions. This is made possible by an adaptive construction of an efficient reduced basis. The proposed approach first initializes a reduced basis during the initial phase of the active learning algorithm. Then, based on a reduced solution accuracy criterion it decides for each point either to use the reduced solution or to solve the full numerical model. As the learning phase of the adaptive sampling concentrates the choice of infill points in the vicinity of the limit state, reduced-basis

	AK-MCS + RB	AK-MCS
computational time of $\boldsymbol{P}^{-1}\boldsymbol{F}$ (once for all)	4.84	-
mean assembly time of $\boldsymbol{K}(\boldsymbol{x})$	86	86
number of evaluations of $G(\boldsymbol{x})$	101	101
number of reduced solutions $\tilde{\boldsymbol{u}}(\boldsymbol{x})$ evaluations	101	101
number of full solutions $\boldsymbol{u}(\boldsymbol{x})$ evaluations	15	
mean time of full solution $\boldsymbol{u}(\boldsymbol{x})$ evaluation	2041	2041
mean time of reduced solution $\tilde{\boldsymbol{u}}(\boldsymbol{x})$ evaluation	1.28	-
mean time of preconditionned residual $\epsilon^P_{RB}(\boldsymbol{x})$ evaluation	2.92	-
total CPU time	39734	214838

Table 12: Operations CPU time (in seconds) for the reliability analysis for the mechanical problem.

modeling may be very efficient as new points are likely to be close to many already computed points. Two different implementations of the approach were proposed, differing in terms of the reduced basis coupling criterion. The applications have highlighted the limitations on a criterion based on a basic residual and the usefulness of an improved criterion based on a preconditioned residual. The performance of the proposed approach was also assessed on the two applications, which have shown that the coupling has a great potential for reducing the computational costs. The speed up is of course dependent of the problem, but on the application problems considered the theoretical speed-up reached up to a factor of 7.1 and the practical speed-up up to a factor of 5.4. As the problems become larger scale in terms of number of degrees of freedom the practical speed-up is expected to increasingly approach the theoretical speed-up. A perspective to improve the coupling criterion is to look at the exploration phase during the learning. Indeed, according to the current definition of the criterion, infill points in less known area are likely to be evaluated using the full numerical model as they are located far from other points. However to clarify

the behaviour of the performance function in less known area due to a high variance reduced solutions may be sufficient in a first step. This consideration could be taken into account in the coupling criterion and may be the subject of a later work.

Acknowledgment

This work was supported by the French National Research Agency (ANR) through the ReBReD project under grant ANR-16-CE10-0002.

Appendix A. Study of Co-kriging reformulations on the thermal problem

Appendix A.1. First reformulation possibility

Due to the high variance of the co-Kriging model and the form of the learning function $U(\boldsymbol{x}) = \frac{|\mu_{\hat{G}}(\boldsymbol{x})|}{\sigma_{\hat{G}}(\boldsymbol{x})}$, the use of co-Kriging for the whole algorithm did not permit an efficient learning. The results obtained on the basis of 20 run of the algorithm with co-Kriging are:

- the learning algorithm converged on average after 231 simulations (on average 40 simulations are needed when using Kriging)
- 4 out of 20 runs were stoped at the 500^{th} iteration

The failure of this strategy can be explained in multiple ways:

- Co-kriging works best when the ratio of the number of low to high fidelity simulations is within a reasonable range, as investigated by Toal [50]. Unfortunately at the beginning of the learning algorithm we are actually very far from this ideal ratio as we have very few reduced basis simulations.
- The problem is not really two-fidelity but n-fidelity. When the reduced basis is enriched the correlation between the reduced basis solution and the full solution may completely change at a new point, compared to a

previously calculated reduced basis solution nearby. This may perturb the co-kriging learning process which sees two points that are very close but that present very different correlations between low and high fidelity.

- The adaptive sampling algorithm for reliability tends to concentrate samples in the close vicinity of the limit state. Most of these samples will be low fidelity reduced basis solutions. This sampling may not be well suited for a reasonable learning of the co-kriging hyperparameters.

Appendix A.2. Second reformulation possibility

The performance of co-Kriging was compared to Kriging by carrying out the following procedure:

- Run of the coupling algorithm using Kriging and saving of high and low-fidelity points
- After convergence of AK-MCS co-Kriging is built using low and high-fidelity points
- Evaluation of the probabilities of failure on a fixed Monte Carlo population using both the Kriging model and the co-Kriging model in order to compare P_f values.

The previous procedure was run 40 times for different initial DoEs and Monte Carlo populations. In order to compare the metamodels the absolute relative differences between the reference probability of failure (Monte Carlo method estimation) and the estimated probability of failure $\frac{|\hat{P}_{f\,MC} - \widehat{P_f}_{AK-MCS+RB}|}{\hat{P}_{f\,MC}}$ were computed for both surrogate models.The following results have been obtained:

	Kriging	co-Kriging
maximal absolute relative difference	0.13	1.15
mean absolute relative difference	0.055	0.27

Table A.13: Second strategy results

We find that the probabilities of failure obtained with the co-Kriging model are on average poorer than with kriging.

We assume that the poor quality of the co-Kriging predictions is due to the first reduced basis solutions (computed with a poor current reduced basis) which are very distant from the true solutions. The issue of varying correlations when the reduced basis is enriched (discussed above for the the first strategy) might also be a major explanation for the poorer quality obtained with co-kriging.

Appendix A.3. Third reformulation possibility

The performance of co-Kriging was compared to Kriging by carrying out the following procedure:

- Run of the coupling algorithm using Kriging and saving of high and low-fidelity points
- After convergence of AK-MCS: re-evaluation of low-fidelity points using the final reduced basis in order to have only two fidelity levels
- Building of co-Kriging using low and high-fidelity points
- Evaluation of the probabilities of failure on a fixed Monte Carlo population using both the Kriging model and the co-Kriging model in order to compare P_f values.

The previous procedure was run 30 times for different initial DoEs and Monte Carlo populations. In order to compare the metamodels the absolute relative differences between the reference probability of failure (Monte Carlo method estimation) and the estimated probability of failure $\frac{|\hat{P_f}_{MC} - \widehat{P_f}_{AK-MCS+RB}|}{\hat{P_f}_{MC}}$ were computed for both surrogate models.The following results have been obtained: The co-Kriging built with this strategy allows to obtain an accurate estimation of the failure probability. However, it can be seen in Table A.14 that the use of co-Kriging does not improve significantly the accuracy of the estimation whereas it increases the computational cost as all reduced basis solutions must be reevaluated. This third strategy may however still be useful for checking that

	Kriging	co-Kriging
maximal absolute relative difference	0.12	0.12
mean absolute relative difference	0.053	0.053

Table A.14: Third strategy results

the final probability of failure estimate obtained with a kriging approach does not differ significantly from the one obtained with a co-kriging approach.

References

[1] R. E. Melchers, A. T. Beck, Structural Reliability Analysis and Prediction, John Wiley & Sons, 2018, google-Books-ID: 8yE6DwAAQBAJ.

[2] E. Vazquez, J. Bect, A sequential Bayesian algorithm to estimate a probability of failure, IFAC Proceedings Volumes 42 (10) (2009) 546–550. doi:10.3182/20090706-3-FR-2004.00090.
URL http://www.sciencedirect.com/science/article/pii/S1474667016387043

[3] B. Echard, N. Gayton, M. Lemaire, N. Relun, A combined Importance Sampling and Kriging reliability method for small failure probabilities with time-demanding numerical models, Reliability Engineering & System Safety 111 (Supplement C) (2013) 232–240. doi:10.1016/j.ress.2012.10.008.
URL http://www.sciencedirect.com/science/article/pii/S0951832012002086

[4] B. J. Bichon, M. S. Eldred, L. P. Swiler, S. Mahadevan, J. M. McFarland, Efficient Global Reliability Analysis for Nonlinear Implicit Performance Functions, AIAA Journal 46 (10) (2008) 2459–2468. doi:10.2514/1.34321.
URL http://arc.aiaa.org/doi/10.2514/1.34321

[5] B. J. Bichon, J. M. McFarland, S. Mahadevan, Efficient surrogate models for reliability analysis of systems with multiple failure modes, Reliability Engineering & System Safety 96 (10) (2011) 1386–1395. doi:10.1016/j.ress.2011.05.008.
URL http://www.sciencedirect.com/science/article/pii/S0951832011001062

[6] W. Fauriat, N. Gayton, AK-SYS: An adaptation of the AK-MCS method for system reliability, Reliability Engineering & System Safety 123 (2014)

137–144. doi:10.1016/j.ress.2013.10.010.
URL http://www.sciencedirect.com/science/article/pii/S0951832013002949

[7] L. Li, J. Bect, E. Vazquez, Bayesian Subset Simulation: a kriging-based subset simulation algorithm for the estimation of small probabilities of failure, in: 11th International Probabilistic Assessment and Management Conference (PSAM11) and The Annual European Safety and Reliability Conference (ESREL 2012), Helsinki, Finland, 2012, pp. CD–ROM Proceedings (10 pages).
URL https://hal-supelec.archives-ouvertes.fr/hal-00715316

[8] V. Dubourg, E. Deheeger, B. Sudret, Metamodel-based importance sampling for the simumation of rare events, in: Faber, M. J. Kohler and K. Nishilima (Eds.), Proceedings of the 11th International Conference of Statistics and Probability in Civil Engineering (ICASP2011), Zurich, Switzerland, 2011.

[9] J. Bect, D. Ginsbourger, L. Li, V. Picheny, E. Vazquez, Sequential design of computer experiments for the estimation of a probability of failure, Statistics and Computing 22 (3) (2012) 773–793. doi:10.1007/s11222-011-9241-4.
URL https://link.springer.com/article/10.1007/s11222-011-9241-4

[10] A. Basudhar, S. Missoum, Reliability assessment using probabilistic support vector machines, International Journal of Reliability and Safety 7 (2) (2013) 156–173. doi:10.1504/IJRS.2013.056378.
URL https://www.inderscienceonline.com/doi/abs/10.1504/IJRS.2013.056378

[11] J.-M. Bourinet, F. Deheeger, M. Lemaire, Assessing small failure probabilities by combined subset simulation and Support Vector Machines, Structural Safety 33 (6) (2011) 343–353.

doi:10.1016/j.strusafe.2011.06.001.
URL http://www.sciencedirect.com/science/article/pii/S0167473011000555

[12] Schöbi R., Sudret B., Marelli S., Rare Event Estimation Using Polynomial-Chaos Kriging, ASCE-ASME Journal of Risk and Uncertainty in Engineering Systems, Part A: Civil Engineering 3 (2) (2017) D4016002. doi:10.1061/AJRUA6.0000870.
URL https://ascelibrary.org/doi/abs/10.1061/AJRUA6.0000870

[13] P. Benner, S. Gugercin, K. Willcox, A Survey of Projection-Based Model Reduction Methods for Parametric Dynamical Systems, SIAM Review 57 (4) (2015) 483–531. doi:10.1137/130932715.
URL http://epubs.siam.org/doi/abs/10.1137/130932715

[14] G. Kerschen, J.-C. Golinval, A. F. Vakakis, L. A. Bergman, The Method of Proper Orthogonal Decomposition for Dynamical Characterization and Order Reduction of Mechanical Systems: An Overview, Nonlinear Dynamics 41 (1-3) (2005) 147–169. doi:10.1007/s11071-005-2803-2.
URL https://link.springer.com/article/10.1007/s11071-005-2803-2

[15] R. E. Melchers, Importance sampling in structural systems, Structural Safety 6 (1) (1989) 3–10. doi:10.1016/0167-4730(89)90003-9.
URL http://www.sciencedirect.com/science/article/pii/0167473089900039

[16] C. Gogu, A. Chaudhuri, C. Bes, How Adaptively Constructed Reduced Order Models Can Benefit Sampling-Based Methodsfor Reliability Analyses, International Journal of Reliability, Quality and Safety Engineering 23 (05) (2016) 1650019.

[17] E. Florentin, P. Díez, Adaptive reduced basis strategy based on goal oriented error assessment for stochastic problems, Computer methods in applied mechanics and engineering 225-228 (2012) 116–127. doi:10.1016/j.

cma.2012.03.016.
URL https://upcommons.upc.edu/handle/2117/116664

[18] S. Boyaval, C. L. Bris, Y. Maday, N. C. Nguyen, A. T. Patera, A reduced basis approach for variational problems with stochastic parameters: Application to heat conduction with variable Robin coefficient, Computer Methods in Applied Mechanics and Engineering 198 (41-44) 3187–3206.
URL http://www.academia.edu/27337716/A_reduced_basis_approach_for_variational_problems_with_stochastic_parameters_Application_to_heat_conduction_with_variable_Robin_coefficient

[19] C. E. Rasmussen, C. K. I. Williams, Gaussian processes for machine learning, Adaptive computation and machine learning, MIT Press, Cambridge, Mass, 2006, oCLC: ocm61285753.

[20] A. I. Forrester, A. J. Keane, Recent advances in surrogate-based optimization, Progress in Aerospace Sciences 45 (1-3) (2009) 50–79. doi:10.1016/j.paerosci.2008.11.001.
URL http://linkinghub.elsevier.com/retrieve/pii/S0376042108000766

[21] B. Echard, N. Gayton, M. Lemaire, AK-MCS: An active learning reliability method combining Kriging and Monte Carlo Simulation, Structural Safety 33 (2) (2011) 145–154. doi:10.1016/j.strusafe.2011.01.002.
URL http://www.sciencedirect.com/science/article/pii/S0167473011000038

[22] X. Huang, J. Chen, H. Zhu, Assessing small failure probabilities by AK–SS: An active learning method combining Kriging and Subset Simulation, Structural Safety 59 (Supplement C) (2016) 86–95. doi:10.1016/j.strusafe.2015.12.003.
URL http://www.sciencedirect.com/science/article/pii/S0167473016000035

[23] N. Lelièvre, P. Beaurepaire, C. Mattrand, N. Gayton, AK-MCSi: A Kriging-based method to deal with small failure probabilities and time-consuming models, Structural Safety 73 (2018) 1–11. doi:10.1016/j.strusafe.2018.01.002.
URL http://www.sciencedirect.com/science/article/pii/S0167473017301558

[24] M. Balesdent, J. Morio, J. Marzat, Kriging-based adaptive Importance Sampling algorithms for rare event estimation, Structural Safety 44 (Supplement C) (2013) 1–10. doi:10.1016/j.strusafe.2013.04.001.
URL http://www.sciencedirect.com/science/article/pii/S0167473013000350

[25] V. Dubourg, B. Sudret, F. Deheeger, Metamodel-based importance sampling for structural reliability analysis, Probabilistic Engineering Mechanics 33 (2013) 47–57. doi:10.1016/j.probengmech.2013.02.002.
URL http://www.sciencedirect.com/science/article/pii/S0266892013000222

[26] F. Cadini, A. Gioletta, A Bayesian Monte Carlo-based algorithm for the estimation of small failure probabilities of systems affected by uncertainties, Reliability Engineering & System Safety 153 (2016) 15–27. doi:10.1016/j.ress.2016.04.003.
URL http://www.sciencedirect.com/science/article/pii/S0951832016300175

[27] F. Cadini, F. Santos, E. Zio, An improved adaptive kriging-based importance technique for sampling multiple failure regions of low probability, Reliability Engineering & System Safety 131 (2014) 109–117. doi:10.1016/j.ress.2014.06.023.
URL http://linkinghub.elsevier.com/retrieve/pii/S0951832014001537

[28] Z. Lv, Z. Lu, P. Wang, A new learning function for Kriging and

its applications to solve reliability problems in engineering, Computers & Mathematics with Applications 70 (5) (2015) 1182–1197. doi:10.1016/j.camwa.2015.07.004.
URL http://www.sciencedirect.com/science/article/pii/S0898122115003399

[29] X. Zhang, L. Wang, J. D. Sørensen, REIF: A novel active-learning function toward adaptive Kriging surrogate models for structural reliability analysis, Reliability Engineering & System Safety 185 (2019) 440–454. doi:10.1016/j.ress.2019.01.014.
URL http://www.sciencedirect.com/science/article/pii/S0951832018305969

[30] Z. Wang, A. Shafieezadeh, REAK: Reliability analysis through Error rate-based Adaptive Kriging, Reliability Engineering & System Safety 182 (2019) 33–45. doi:10.1016/j.ress.2018.10.004.
URL http://www.sciencedirect.com/science/article/pii/S0951832017312504

[31] B. Gaspar, A. P. Teixeira, C. Guedes Soares, Adaptive surrogate model with active refinement combining Kriging and a trust region method, Reliability Engineering & System Safety 165 (2017) 277–291. doi:10.1016/j.ress.2017.03.035.
URL http://www.sciencedirect.com/science/article/pii/S0951832016301892

[32] G. Perrin, Active learning surrogate models for the conception of systems with multiple failure modes, Reliability Engineering & System Safety 149 (2016) 130–136. doi:10.1016/j.ress.2015.12.017.
URL http://www.sciencedirect.com/science/article/pii/S0951832015003695

[33] B. Peherstorfer, K. Willcox, M. Gunzburger, Survey of multifidelity methods in uncertainty propagation, inference, and optimization, SIAM

Review 60 (3) (2018) 550–591. doi:10.1137/16M1082469.
URL https://nyuscholars.nyu.edu/en/publications/survey-of-multifidelity-methods-in-uncertainty-propagation-infere

[34] D. G. Krige, A statistical approach to some basic mine valuation problems on the Witwatersrand, Journal of the Southern African Institute of Mining and Metallurgy 52 (6) (1951) 119–139.
URL https://journals.co.za/content/saimm/52/6/AJA0038223X_4792

[35] G. Matheron, Principles of geostatistics, Economic Geology 58 (8) (1963) 1246–1266. doi:10.2113/gsecongeo.58.8.1246.
URL https://pubs.geoscienceworld.org/segweb/economicgeology/article-abstract/58/8/1246/17275/principles-of-geostatistics

[36] D. R. Jones, A Taxonomy of Global Optimization Methods Based on Response Surfaces, Journal of Global Optimization 21 (4) (2001) 345–383. doi:10.1023/A:1012771025575.
URL https://doi.org/10.1023/A:1012771025575

[37] B. I. A.-L. P. Michaël Baudin, Anne Dutfoy, Openturns: An industrial software for uncertainty quantification in simulation.

[38] K. Smetana, O. Zahm, A. Patera, Randomized Residual-Based Error Estimators for Parametrized Equations, SIAM Journal on Scientific Computing 41 (2) (2019) A900–A926. doi:10.1137/18M120364X.
URL https://epubs.siam.org/doi/abs/10.1137/18M120364X

[39] G. Rozza, D. B. P. Huynh, A. T. Patera, Reduced Basis Approximation and a Posteriori Error Estimation for Affinely Parametrized Elliptic Coercive Partial Differential Equations: Application to Transport and Continuum Mechanics, Archives of Computational Methods in Engineering 15 (3) (2008) 229–275. doi:10.1007/s11831-008-9019-9.
URL http://link.springer.com/10.1007/s11831-008-9019-9

[40] A. Janon, M. Nodet, C. Prieur, C. Prieur, Goal-oriented error estimation for fast approximations of nonlinear problems, Research Report, GIPSA-lab (2016).
URL https://hal.archives-ouvertes.fr/hal-01290887

[41] T. Tonn, K. Urban, S. Volkwein, Comparison of the reduced-basis and POD *a posteriori* error estimators for an elliptic linear-quadratic optimal control problem, Mathematical and Computer Modelling of Dynamical Systems 17 (4) (2011) 355–369. doi:10.1080/13873954.2011.547678.
URL http://www.tandfonline.com/doi/abs/10.1080/13873954.2011.547678

[42] C. Gogu, J.-C. Passieux, Efficient surrogate construction by combining response surface methodology and reduced order modeling, Structural and Multidisciplinary Optimization 47 (6) (2013) 821–837. doi:10.1007/s00158-012-0859-4.
URL https://link.springer.com/article/10.1007/s00158-012-0859-4

[43] O. Zahm, A. Nouy, Interpolation of inverse operators for preconditioning parameter-dependent equations, SIAM Journal on Scientific Computing 38 (2) (2016) A1044–A1074.

[44] R. G. Ghanem, R. M. Kruger, Numerical solution of spectral stochastic finite element systems, Computer Methods in Applied Mechanics and Engineering 129 (3) (1996) 289–303. doi:10.1016/0045-7825(95)00909-4.
URL http://www.sciencedirect.com/science/article/pii/0045782595009094

[45] O. Zahm, M. Billaud-Friess, A. Nouy, Projection based model order reduction methods for the estimation of vector-valued variables of interest, arXiv:1603.00336 [math]ArXiv: 1603.00336.
URL http://arxiv.org/abs/1603.00336

[46] J. Riccius, O. Haidn, E. Zametaev, Influence of Time Dependent Effects on the Estimated Life Time of Liquid Rocket Combustion Chamber Walls, in: 40th AIAA/ASME/SAE/ASEE Joint Propulsion Conference and Exhibit, American Institute of Aeronautics and Astronautics. doi:10.2514/6.2004-3670.
URL https://arc.aiaa.org/doi/abs/10.2514/6.2004-3670

[47] J. Riccius, E. Zametaev, O. Haidn, C. Gogu, LRE Chamber Wall Optimization Using Plane Strain and Generalized Plane Strain Models, in: 42nd AIAA/ASME/SAE/ASEE Joint Propulsion Conference & Exhibit, American Institute of Aeronautics and Astronautics. doi:10.2514/6.2006-4366.
URL https://arc.aiaa.org/doi/abs/10.2514/6.2006-4366

[48] A. J. M. Ferreira, MATLAB Codes for Finite Element Analysis, Solid Mechanics and Its Applications, Springer Netherlands, 2009.
URL //www.springer.com/gp/book/9781402091995

[49] Electricité de france *Finite element code_ aster, Analysis of Structures and Thermomechanics for Studies and Research*, open source on www.code-aster.org, 1989–2017.

[50] D. J. Toal, Some considerations regarding the use of multi-fidelity kriging in the construction of surrogate models, Structural and Multidisciplinary Optimization 51 (6) (2015) 1223–1245.